J. Fluid Mech. (2012), *vol.* 710, *pp.* 362–378.
doi:10.1017/jfm.2012.367

Particle capture and low-Reynolds-number flow around a circular cylinder

Alexis Espinosa-Gayosso[1,2]†, Marco Ghisalberti[1], Gregory N. Ivey[1,2] and Nicole L. Jones[1,2]

[1] School of Environmental Systems Engineering, University of Western Australia, Crawley, WA 6009, Australia

[2] UWA Oceans Institute, University of Western Australia, Crawley, WA 6009, Australia

(Received 21 December 2011; revised 22 May 2012; accepted 18 July 2012; first published online 7 September 2012)

Particle capture, whereby suspended particles contact and adhere to a solid surface (a 'collector'), is an important mechanism in a range of environmental processes. In aquatic systems, typically characterized by low collector Reynolds numbers (Re), the rate of particle capture determines the efficiencies of a range of processes such as seagrass pollination, suspension feeding by corals and larval settlement. In this paper, we use direct numerical simulation (DNS) of a two-dimensional laminar flow to accurately quantify the rate of capture of low-inertia particles by a cylindrical collector for $Re \leqslant 47$ (i.e. a range where there is no vortex shedding). We investigate the dependence of both the capture rate and maximum capture angle on both the collector Reynolds number and the ratio of particle size to collector size. The inner asymptotic expansion of Skinner (*Q. J. Mech. Appl. Maths*, vol. 28, 1975, pp. 333–340) for flow around a cylinder is extended and shown to provide an excellent framework for the prediction of particle capture and flow close to the leading face of a cylinder up to $Re = 10$. Our results fill a gap between theory and experiment by providing, for the first time, predictive capability for particle capture by aquatic collectors in a wide (and relevant) Reynolds number and particle size range.

Key words: low-Reynolds-number flows, particle/fluid flow, suspensions

1. Introduction

The term 'particle capture' refers to the physical process by which suspended particles come into contact with a solid structure ('collector') and adhere to the collector's surface, as shown in figure 1. One important example of particle capture in aquatic systems is the adhesion of particles to aquatic vegetation surfaces, a phenomenon which defines the filtration and water purification capacity of vegetated wetlands. Particle capture is also of significant ecological importance in marine ecosystems; in particular, it controls the efficiency of seagrass pollination, suspension feeding (of e.g. corals), and larval settlement. Despite its fundamental ecological importance, predictive capability for the rate of particle capture in aquatic systems is lacking.

† Email address for correspondence: Alexis.Espinosa.Gayosso@gmail.com

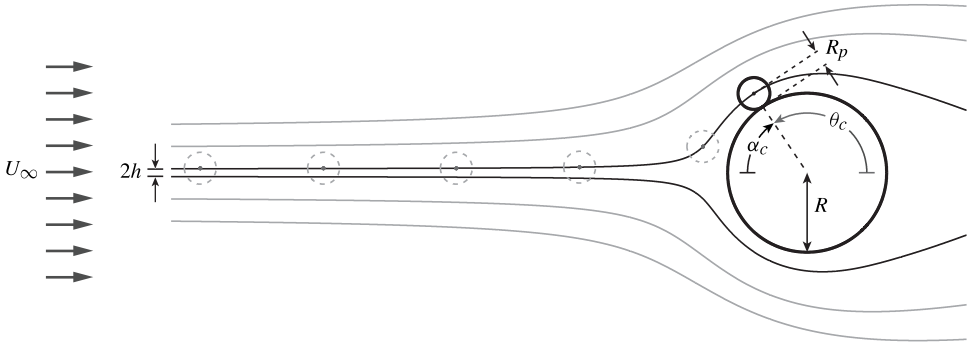

FIGURE 1. Direct interception of low-inertia particles, whose trajectories match that of the streamlines, in uniform steady flow. The maximum angle of capture (α_c or θ_c, depending on the coordinate system used) is indicated by the dotted line within the collector. The trajectory of a particle captured at the maximum angle of capture is shown; the streamline followed by the particle centre defines the limiting streamline. The separation between limiting streamlines upstream of the influence of the cylindrical collector ($2h$) is used to define the capture efficiency η_{DI} (1.8).

For simplicity, collectors such as vegetation stems or the capturing filaments of suspension feeders are often modelled as cylinders and particles as spheres. The capture efficiency (η) of a cylindrical collector can be defined as the ratio of the number of particles captured (N_c) to the number of particles whose centres would have passed through the space occupied by the collector were it not present in the flow (N_a):

$$\eta = \frac{N_c}{N_a}. \tag{1.1}$$

Here we consider perfect particle–collector adhesion, such that all particles are assumed to be captured when they contact the cylinder surface.

In general, capture efficiency depends on four parameters,

$$\eta = \eta(r_p, \rho^+, Re, Pe), \tag{1.2}$$

where r_p is the particle size ratio, ρ^+ is the particle density ratio, Re is the Reynolds number of the collector and Pe is the Péclet number for particle transport. The definition of each of these parameters is as follows:

$$r_p = \frac{D_p}{D} \equiv \frac{R_p}{R}, \tag{1.3}$$

$$\rho^+ = \frac{\rho_p}{\rho}, \tag{1.4}$$

$$Re = \frac{\rho U_\infty D}{\mu}, \tag{1.5}$$

$$Pe = \frac{U_\infty D}{\Gamma_p}, \tag{1.6}$$

where D_p and R_p are the particle diameter and radius, D and R are the collector diameter and radius, ρ_p is the particle density, ρ is the fluid density, U_∞ is the uniform upstream fluid velocity, μ is the fluid viscosity and Γ_p is the particle diffusivity. The

values of these parameters define the relative importance of three different mechanisms of particle capture (Friedlander 2000): (i) inertial impaction, where particle inertia causes deviation from fluid streamlines and contact with the collector; (ii) diffusional deposition, where particle–collector contact is driven by random motions (such as Brownian motion); and (iii) direct interception, where particle centres follow the streamlines and contact is made due to the finite particle size.

Inertial impaction is typically neglected in aquatic systems due to the low Stokes numbers (St) of suspended particles. The Stokes number, which represents the importance of particle inertia, is defined as:

$$St = \frac{\rho_p D_p^2 U_\infty}{18\mu} = \frac{\rho^+ r_p^2 Re}{18} \tag{1.7}$$

(Friedlander 2000). Particle inertia can be neglected when St is below a critical value $St_c \sim O(0.1)$ that varies slightly with Re (Phillips & Kaye 1999). As St is typically small in the aquatic systems of interest (due in part to the fact that $\rho^+ \approx 1$, (Harvey, Bourget & Ingram 1995; Shimeta & Koehl 1997; Ackerman 1997, 2006)), direct interception has been recognized as the more important capture mechanism (Rubenstein & Koehl 1977; Shimeta & Jumars 1991; Wildish & Kristmanson 1997; Palmer *et al.* 2004).

Capture due to Brownian diffusion is also small relative to direct interception unless both Re and Pe are small (Friedlander 1967). For example, diffusional deposition on oceanic suspension feeders only becomes important when $D_p \lesssim O(1\ \mu\text{m})$ (Shimeta 1993).

Here we investigate direct interception of low-inertia particles by circular cylinder collectors. It is assumed that the particles follow streamlines exactly and have a negligible influence on the flow field. Particles are captured if their streamline comes within one particle radius of the collector. The outermost streamline that permits capture of a particle of radius R_p is the 'limiting streamline' for that particle (figure 1). For any given particle size, there are two limiting streamlines for the symmetrical flow around a cylinder; all suspended particles that approach the cylinder with their centres on or between these two limiting streamlines will be captured, while no particles with centres outside the limiting streamlines will reach the collector surface. The capture efficiency by direct interception (η_{DI}) can thus be defined as

$$\eta_{DI} = \frac{2h}{D} \equiv \frac{h}{R}, \tag{1.8}$$

where $2h$ is the minimum distance between the limiting streamlines upstream of the cylinder. The radial velocity of any captured particle will be negative (i.e. towards the cylinder surface) throughout its trajectory. On the other hand, a non-captured particle may approach the cylinder but, as soon as its radial velocity becomes positive, it can no longer be captured. Therefore, particles will be captured on the front of the collector within $-\alpha_c \leqslant \alpha \leqslant \alpha_c$, where α_c is the maximum angle of capture, determined by the point at which the radial velocity changes from negative to positive at a distance R_p from the cylinder surface. This point also defines the limiting streamline (figure 1). (Here, α is used for angles measured clockwise from the frontal stagnation point, while θ is used for angles measured anticlockwise from the lee-side stagnation point, as shown in figure 1.)

The capture efficiency, together with the upstream fluid velocity and the size of the collector, defines the rate at which particles are captured on the collector surface. For a

Collector	Particle	D (μm)	D_p (μm)	U_∞ (cm s^{-1})	Reference
Soft coral tentacle	Plankton	300	100	20	Wildish & Kristmanson (1997)
Red algae branch	Larvae	1000	200	5	Harvey *et al.* (1995)
Seagrass stigma	Pollen	100	100	50	Ackerman (1997, 2006)
Wetland vegetation	Sediment	5000	200	1	Palmer *et al.* (2004)

TABLE 1. Typical collector and particle sizes in relevant aquatic ecosystems. The upstream velocities for which $Re \approx 47$ are also indicated.

given concentration of particles C_p, the rate of capture is given by

$$\frac{\mathrm{d}N_c}{\mathrm{d}t} = \eta_{DI} C_p U_\infty D l, \tag{1.9}$$

where t is time and l is the axial length of the collector. If the flow field is known exactly, limiting streamlines can be determined and the capture efficiency and capture rate calculated.

The description of low-Reynolds-number flow around a circular cylinder has long been a focus of analytical research in fluid mechanics (e.g. Stokes 1851; Oseen 1910; Lamb 1911; Davies 1950; Kaplun 1957; Proudman & Pearson 1957; Skinner 1975; Keller & Ward 1996; Veysey & Goldenfeld 2007). Based on drag coefficient estimates, existing analytical predictions of the flow field around a cylinder have limited validity above $Re \approx 1$ (Lange, Durst & Breuer 1998; Veysey & Goldenfeld 2007). However, particle capture in aquatic systems is not necessarily limited to very low Re. Here, we aim to describe particle capture for all Reynolds numbers below the onset of vortex shedding ($Re \leqslant 47$), a range highly relevant to the aquatic systems of interest (table 1). Previous estimation of direct interception efficiency by a single cylinder has relied mostly on the creeping flow solution of Lamb (1911), a solution which has been applied to particle capture in aquatic environmental systems (Shimeta 1993; Wildish & Kristmanson 1997). This solution, however, leads to inaccurate estimation of the capture efficiency when $Re \gtrsim 1$ (Friedlander 1967). While there are a small number of experimental and numerical studies that explore the capture of low-inertia particles by circular cylinders for $Re \sim O(1\text{–}10)$ (Davies & Peetz 1956; Palmer *et al.* 2004; Humphries 2009; Haugen & Kragset 2010), they do not describe particle capture across the entire Reynolds number and particle size ranges of interest.

In this paper, we have used direct numerical simulation (DNS) of flow around a cylinder to provide predictive capability for particle capture in aquatic systems. In particular, we have quantified the dependence of the capture efficiency on the particle size ratio and on the Reynolds number. We will demonstrate the limit of validity of prior theoretical approximations and show that the analytical solution of Skinner (1975) for the flow field around a cylinder at low Re can be extended, for the purposes of particle capture prediction, to $Re = 10$.

2. Analytical solutions of low-*Re* flow close to a circular cylinder

As mentioned in § 1, analytical solutions exist for low-Re flow around a cylinder but they are not applicable to the full range of Re considered here. In this section, we present a brief description of the mathematical formulation of flow around a cylinder,

the creeping flow solution of Lamb (1911) for $Re \ll 1$, and the inner asymptotic expansion of the solution by Skinner (1975).

2.1. *Mathematical formulation*

Two-dimensional, unbounded, incompressible and steady low-*Re* flow around a circular cylinder, is sketched in figure 1. The non-dimensional continuity and Navier–Stokes equations for this flow are

$$\boldsymbol{\nabla} \cdot \boldsymbol{u} = 0 \tag{2.1}$$

and

$$(\boldsymbol{\nabla u})\boldsymbol{u} = -\boldsymbol{\nabla} p + \frac{1}{\epsilon}\nabla^2 \boldsymbol{u}, \tag{2.2}$$

where $\boldsymbol{u}$ is the non-dimensional velocity vector, p is the non dimensional pressure and ϵ is the Reynolds number using U_∞ and R as the velocity and length scales, respectively. Therefore

$$\epsilon = \frac{\rho U_\infty R}{\mu} = \tfrac{1}{2} Re. \tag{2.3}$$

Defining (r, θ) as the non-dimensional cylindrical coordinates with the origin at the centre of the cylinder, the radial (u_r) and tangential (u_θ) velocity components can be written in terms of the non-dimensional stream function $\psi = \psi(r, \theta; \epsilon)$ as

$$u_r = \frac{1}{r}\frac{\partial \psi}{\partial \theta} \quad \text{and} \quad u_\theta = -\frac{\partial \psi}{\partial r}. \tag{2.4}$$

The boundary conditions are the no-slip condition at the cylinder surface

$$(u_r, u_\theta) = (0, 0) \quad \text{at } r = 1, \tag{2.5}$$

and a uniform horizontal free-stream flow far from the cylinder

$$(u_r, u_\theta) \to (\cos\theta, -\sin\theta) \quad \text{as } r \to \infty. \tag{2.6}$$

2.2. *Creeping flow solution*

Lamb (1911) obtained the first approximate analytical solution of flow around a cylinder using the simplified version of (2.2) proposed by Oseen (1910), in which inertial forces are neglected close to the cylinder but not away from it (in the region of uniform flow). An inner expansion of his solution valid close to the cylinder ($r \lesssim 1/\epsilon$) can be written as

$$\psi_L(r, \theta; \epsilon) = \delta(\epsilon)\left(r \ln r - \frac{r}{2} + \frac{1}{2r}\right)\sin\theta \tag{2.7}$$

(Proudman & Pearson 1957), where δ is a small parameter defined in terms of ϵ as

$$\delta(\epsilon) \equiv \frac{1}{\ln 4 - \gamma - \ln\epsilon + 1/2}, \tag{2.8}$$

and $\gamma = 0.5772$ is Euler's constant. The stream function (2.7) depends on ϵ via δ and is only valid for $Re \ll 1$.

2.3. *Inner asymptotic solution*

Skinner (1975) obtained a higher-order inner asymptotic expansion to describe the flow field around a cylinder, following the work of Kaplun (1957) and Proudman & Pearson (1957). The first two terms of the inner asymptotic expansion are

$$\begin{aligned}\psi_S(r,\theta;\epsilon) = a(\delta)\left(r\ln r - \frac{r}{2} + \frac{1}{2r}\right)\sin\theta \\ + \epsilon\left[\frac{a^2(\delta)}{32}\left(2r^2\ln^2 r - r^2\ln r + \frac{r^2}{4} - \frac{1}{4r^2}\right)\right. \\ \left. + \frac{b(\delta)}{8}\left(r^2 - 2 + \frac{1}{r^2}\right)\right]\sin 2\theta + O\left(\epsilon^2\right),\end{aligned} \tag{2.9}$$

where $a(\delta)$ and $b(\delta)$ are parameters of integration which allow the solution to be matched to an asymptotic outer expansion. The values of a and b depend on ϵ via δ (2.8), and are given by

$$a(\delta) = \delta - 0.8669\delta^3 + O(\delta^5) \quad \text{and} \quad b(\delta) = -1/2 + \delta/4 + O(\delta^2) \tag{2.10}$$

(Kaplun 1957; Skinner 1975). The asymptotic inner expansion (2.9) is valid close to the cylinder ($r \lesssim 1/\epsilon$). The corresponding drag coefficient obtained from the inner asymptotic solution ((2.9) and (2.10)) is the same as the one obtained by Kaplun (1957) and is accurate for $Re \lesssim 1$ (Lange *et al.* 1998; Veysey & Goldenfeld 2007). In this study, we extend the applicability of (2.9) up to $Re = 10$ by using a hybrid approach for obtaining the values of a and b, instead of the series in (2.10). A detailed description of our hybrid approach is presented in § 3.

3. Hybrid approach for extending the applicability of the inner asymptotic expansion

As discussed in § 2.3, the inner asymptotic solution ((2.9) and (2.10)) is not valid and hence inaccurate for $Re \gtrsim 1$ ($\epsilon \gtrsim 0.5$). This inaccuracy arises from two problems: (i) the truncation of the series for a and b in (2.10); and (ii) the divergence induced by the existence of a singular point in the definition of δ (2.8) at $Re = 7.405$. Keller & Ward (1996) suggested avoiding the first problem through a hybrid method that matches the inner asymptotic expansion (2.9) to a numerical solution of the outer flow, in an effort to allow a and b to be obtained to all orders of δ and thus extend the validity of (2.9) up to $Re = 4$. Unfortunately, their reported values of a and b do not generate the correct flow field, as will be shown below. Our hybrid approach avoids the two problems mentioned above by using a DNS of the full Navier–Stokes and continuity equations in a wide domain that includes the inner flow (i.e. adjacent to the cylinder surface). This hybrid approach allows accurate description of a and b and therefore of the flow field around the cylinder for $Re \sim O(1\text{–}10)$.

3.1. *Numerical methods and boundary conditions*

The steady, incompressible and two-dimensional equations of motion ((2.1) and (2.2)) were solved with the finite-volume method (Ferziger & Perić 2002) using the open source code OpenFOAM (2012). The velocity and pressure coupling was solved with the SIMPLE iterative algorithm (Patankar 1980). Convergence was deemed to be satisfied when the initial residuals of the pressure and momentum equations fell below 5×10^{-11}.

Although we consider an unbounded flow, the solver requires boundaries a finite distance from the cylinder. For simulation of low-Re flow, computational domains need to be extremely large to avoid blockage effects (Lange *et al.* 1998; Posdziech & Grundmann 2007). Simulations were performed with the cylinder at the centre of a square domain of side length L. The length of the domain always satisfied $L/D > 4000Re^{-0.8}$, reducing the blockage effect error to less than an estimated 0.1 % (Lange *et al.* 1998). As the flow is steady and symmetrical for $Re \leqslant 47$, the solution was limited to the upper half of the domain. The domain around the cylinder surface ($r = 1$) was discretized with an O-type grid ($1 \leqslant r \leqslant 1.2$) coupled smoothly with an H-type grid which extended over the rest of the domain ($r \gtrsim 2.6$) (similar to the mesh topology used by Wu *et al.* 2004). Grid points were concentrated around the cylinder and in the wake region. The size of the cell closest to the cylinder wall was $\Delta r = 10^{-3}$ and a total of 372 cells were used to discretize the half-cylinder perimeter.

The no-slip boundary condition, $(u_r, u_\theta) = (0, 0)$, was applied at the surface of the cylinder and the outflow condition, $(\boldsymbol{\nabla u})\boldsymbol{n} = 0$ (where $\boldsymbol{n}$ is a unit vector normal to the boundary), was applied at the downstream boundary. The velocity at the upstream boundary was fixed at the free-stream value, $(u_r, u_\theta) = (\cos\theta, -\sin\theta)$, and the lateral boundary was treated as a no-flux free-slip surface. The pressure was set to zero at the outflow boundary and a Neumann-type condition was used for pressure along all other boundaries. As we only solved for the flow in one half of the domain, symmetry boundary conditions for all variables were applied at the plane of symmetry.

3.2. *Validation of the numerical solutions*

Our DNS ($0.01 \leqslant Re \leqslant 47$) were validated by comparing both the cylinder drag coefficient ($C_D = 2F_D/\rho U_\infty^2 D$ where F_D is the drag force on the cylinder per unit length) and the angle of separation (α_s) to existing analytical, experimental and numerical data. The numerical values of C_D agree very well with: (i) the analytical drag coefficients obtained from theoretical solutions within their range of validity; (ii) the experimental measurements of Tritton (1959) and Huner & Hussey (1977) for $Re \gtrsim 0.2$; and (iii) the DNS of Posdziech & Grundmann (2007) for $Re \geqslant 5$ (figure 2*a*).

Flow separation from the cylinder surface occurs when $Re \gtrsim 7$ (Wu *et al.* 2004). The separation angle obtained from our DNS agrees almost exactly with the numerical and experimental values of Wu *et al.* (2004) (figure 2*b*).

3.3. *Values of a and b for the hybrid approach*

The parameters a and b in the asymptotic inner expansion (2.9) were calculated by performing a least-squares fit of (2.9) to the numerical flow field for $0.01 \leqslant Re \leqslant 10$. Our values of a and b converge towards the theoretical series (2.10) as the Reynolds number decreases (figure 3), validating the hybrid approach. As expected, our values of a and b are well-behaved and finite for $Re > 1$. While the Keller & Ward (1996) values of a agree with our results and with theory, their values of b do not and generate an erroneous velocity field for $Re > 1$ (see § 4.2). The expressions

$$a(\sigma) \approx 0.148 + 2.15 \times 10^{-2}\sigma + 3.05 \times 10^{-3}\sigma^2 + 2.13 \times 10^{-4}\sigma^4, \tag{3.1a}$$

$$b(\sigma) \approx -0.462 + 5.73 \times 10^{-3}\sigma + 8.65 \times 10^{-4}\sigma^3 - 7.45 \times 10^{-6}\sigma^5, \tag{3.1b}$$

where $\sigma = \ln(Re) - \ln(0.01)$, provide values of a and b within 1.5 % of the DNS estimates for $0.01 \leqslant Re \leqslant 10$. The first two terms of each fit in (3.1) coincide

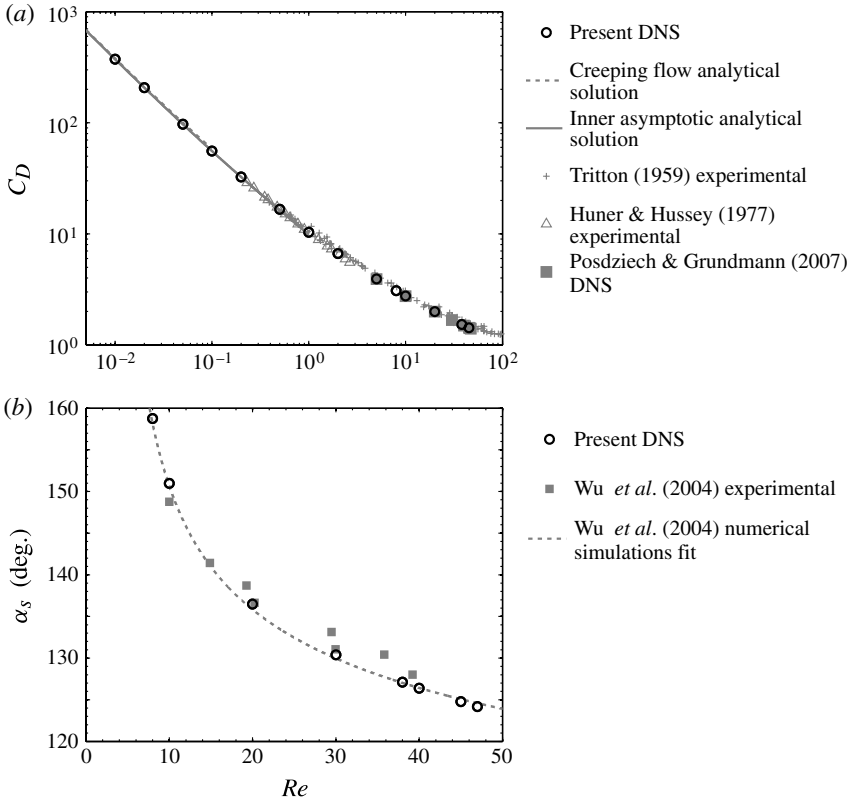

FIGURE 2. The agreement of the present DNS with existing analytical, experimental and numerical data. (*a*) Drag coefficient C_D. (*b*) Separation angle α_s. Note that α_s is measured from the frontal stagnation point.

with the corresponding terms of a Taylor series expansion of the theoretical values (2.10) around $\sigma = 0$. We show below that our values of a and b provide an accurate description of the flow, and of particle capture, up to $Re = 10$.

3.4. *Limits of validity of the hybrid approach*

The values of a and b obtained with our hybrid approach (figure 3) together with expression (2.9) are able to accurately represent the flow around the entire cylinder for $Re \leqslant 1$ (figure 4*a*). Streamlines from the DNS and the hybrid approach are almost indistinguishable within the radial zone $r \lesssim 1/\epsilon$ for all angles (shaded zone). For $1 < Re \leqslant 10$, the hybrid approach is able to accurately represent the flow around the leading face of the cylinder (the region of interest for particle capture) but not on the lee side (figure 4*b*). This behaviour is not a failure of the fitting process, but a characteristic of the analytical inner asymptotic expansion (2.9) which returns to the uniform flow condition faster than the real flow. In the range $1 < Re \leqslant 10$, our hybrid approach is accurate for $r \lesssim 1 + 1/\epsilon$ and $-90° \leqslant \alpha \leqslant 90°$, with an error of less than 3 % with respect to the validated DNS. The hybrid approach is not applicable for $Re > 10$.

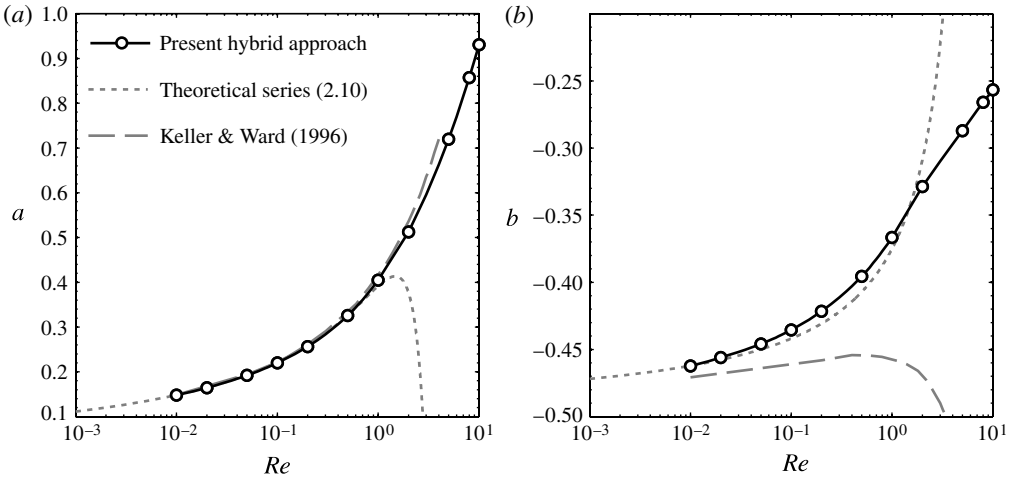

FIGURE 3. Dependence on Re of the parameters (*a*) a and (*b*) b to be used in (2.9) for the hybrid approach. Circles indicate the Reynolds numbers at which DNS were performed.

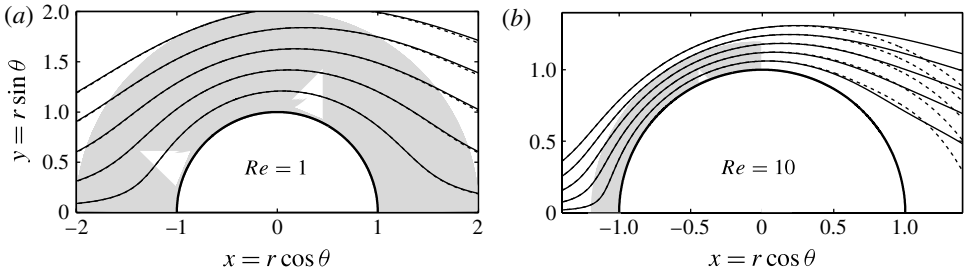

FIGURE 4. Comparison of streamlines from DNS (solid lines) and the hybrid approach (dashed lines) for: (*a*) $Re = 1$; and (*b*) $Re = 10$. The shaded grey area shows the zone of validity of the hybrid approach.

4. Particle capture

In this section, we quantify the maximum angle of capture and the capture efficiency by direct interception. As low-inertia particles are assumed to follow streamlines exactly, obtaining particle trajectories by integration of the particle equation of motion is not necessary and the capture analysis was performed through examination of the fluid velocity field. This methodology assumes that particle forces such as lift (induced by shear), van der Waals attraction and hydrodynamic repulsion to contact may be neglected to leading order, and we test this by comparing our particle capture estimates against low-Re theory and experiments at higher Reynolds numbers.

4.1. *Maximum angle of capture: theoretical considerations*

Knowledge of the angle at which the radial velocity changes sign (θ_c or α_c, figure 1) at a distance R_p from the cylinder surface is required to estimate the particle capture efficiency because it coincides with the maximum angle of capture of zero-inertia

particles, as explained in § 1. Hence, θ_c can be obtained from the implicit equation

$$u_r(r = 1 + r_p, \theta = \theta_c) = 0, \tag{4.1}$$

which can be applied to numerical or analytical solutions of the non-dimensional problem defined in § 2.1.

Of special interest is the maximum angle of capture (θ_{c0}) of particles with a vanishing size ratio ($r_p \to 0$). This angle cannot be obtained from (4.1) because $u_r \to 0$ as $r_p \to 0$ for all θ. However, θ_{c0} can be obtained using the fact that

$$\left.\frac{\partial u_r}{\partial r}\right|_{r=1} = 0, \tag{4.2}$$

which is a consequence of the conservation of mass (2.1), rewritten as

$$\frac{\partial u_r}{\partial r} + \frac{u_r}{r} + \frac{1}{r}\frac{\partial u_\theta}{\partial \theta} = 0, \tag{4.3}$$

and the no-slip condition at the cylinder surface (2.5), which implies

$$u_r = 0, \quad u_\theta = 0, \quad \frac{\partial u_r}{\partial \theta} = 0 \quad \text{and} \quad \frac{\partial u_\theta}{\partial \theta} = 0 \quad \forall\theta \text{ at } r = 1. \tag{4.4}$$

Therefore, the radial velocity reaches either a maximum or a minimum at the surface depending on its sign close to the cylinder, as implied by (4.2). The sign of the second derivative at the surface can be used to determine if the zero radial velocity represents a maximum or a minimum but, at θ_{c0}, the second derivative also changes sign because there is a switch from maximum to minimum, hence

$$\left.\frac{\partial^2 u_r}{\partial r^2}\right|_{\{r=1,\theta=\theta_{c0}\}} = 0. \tag{4.5}$$

Use of (4.5) together with the creeping flow solution (2.7) yields a constant $\theta_{c0} = 90^\circ$ in this limit. More accurate values of θ_{c0} can be obtained by substituting the inner asymptotic expansion (2.9) into (4.5), and solving the resulting implicit equation:

$$2a\cos\theta_{c0} + 2b\epsilon\cos 2\theta_{c0} = 0. \tag{4.6}$$

Note that θ_{c0} also coincides with the angle of maximum vorticity (and maximum gradient of tangential velocity) at the cylinder surface.

4.2. *Maximum angle of capture: results*

The angle θ_{c0} at which the radial velocity close to the cylinder changes sign was obtained directly from the numerical simulations for $0.01 \leqslant Re \leqslant 47$ and is in strong agreement with both theory and experiment (see figure 5*a* and note that $\alpha_{c0} = 180^\circ - \theta_{c0}$). The numerical results agree with the theoretical values of Skinner (1975) ((2.10) and (4.6)) within that study's range of validity, and $\alpha_{c0} \to 90^\circ$ as $Re \to 0$, in agreement with creeping flow theory (Lamb 1911). Note that α_{c0} decreases with Re and reaches $\alpha_{c0} \approx 50^\circ$ for $Re = 47$. This agrees with the angle of maximum vorticity found by Sen, Mittal & Biswas (2009) in their numerical analysis for $Re = 20$ and with the experimental work of Palmer *et al.* (2004), who reported a constant maximum capturing angle of $\alpha_{c0} \approx 50^\circ$ for their low-inertia particle capture experiments in the range $38 \leqslant Re \leqslant 486$.

The predictions of the maximum angle of capture of particles of vanishing size ratio (θ_{c0}) from the hybrid approach (values of a and b taken from (3.1) together

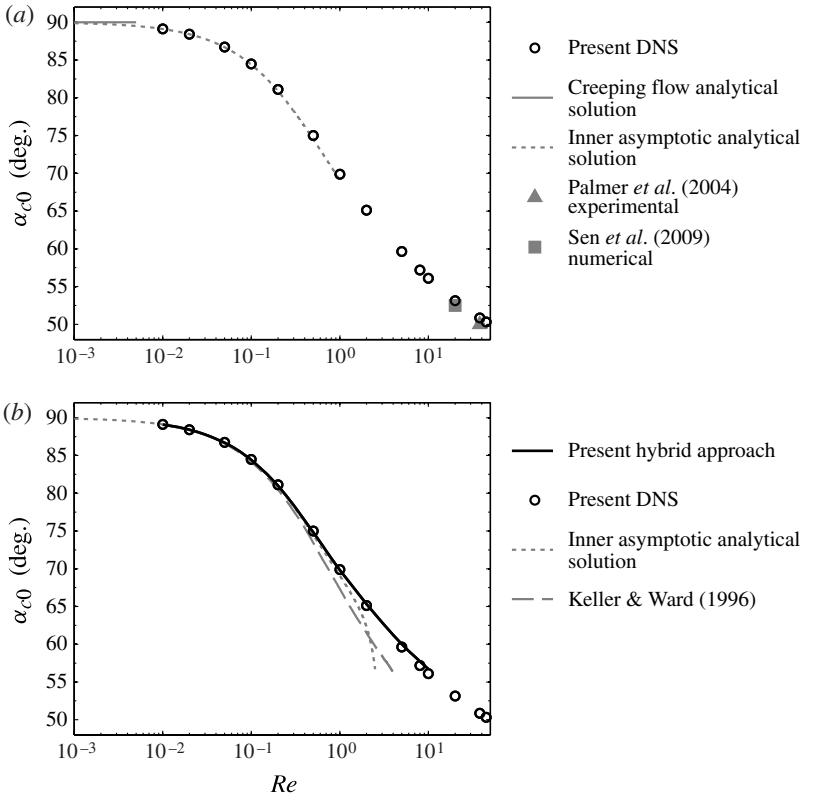

FIGURE 5. Angle of change of sign of the radial velocity close to the frontal cylinder surface (α_{c0}) as a function of Re. This angle coincides with the maximum angle of capture of particles of vanishing size ratio over the frontal face of the cylinder, and with the point of maximum gradient of tangential velocity at the surface. (*a*) The agreement of the present DNS with existing theoretical, experimental and numerical data. (*b*) The agreement of the hybrid approach with the DNS results for $Re \leqslant 10$. Existing hybrid and theoretical solutions are plotted to demonstrate their inaccuracy above $Re = 1$.

with (4.6)) agree very well with the numerical results for $Re \leqslant 10$ (figure 5*b*). Previous analytical expressions give accurate results over more restricted ranges of Re. The capture angle in creeping flow ($\alpha_{c0} = 90°$) is valid only for $Re < 0.001$. The values of a and b obtained by Keller & Ward (1996) do not accurately predict θ_{c0} and, consequently, the flow close to the cylinder for $Re \gtrsim 1$. In summary, our hybrid approach correctly describes the flow around the frontal face of the cylinder and can be used for estimating θ_c and θ_{c0} over a much wider range of Re than existing techniques.

4.3. *Particle capture efficiency: theoretical considerations*

The definition of the capture efficiency by direct interception (1.8) can be interpreted as a ratio of flow rates in one half of the symmetrical domain (see figure 1). Specifically,

$$\eta_{DI} = \frac{Q_h}{Q_R} = \frac{q_h}{q_R} = q_h, \tag{4.7}$$

where $Q_h = U_\infty hl$ is the flow rate between the limiting streamline and the symmetry streamline ($\psi = 0$), and $Q_R = U_\infty Rl$ is the flow rate directly approaching the cylinder. When analysing the solution of the non-dimensional problem defined in § 2.1, the capture efficiency (4.7) can be obtained with the non-dimensional flow rates $q_h = Q_h/Q_R = h/R$ and $q_R = Q_R/Q_R = 1$ and the capture efficiency can therefore be estimated directly from q_h. As the flow rate between streamlines is constant, q_h can be obtained by integrating the tangential velocity profile at $\theta = \theta_c$ (the maximum angle of capture defined by (4.1)) from the cylinder surface ($\psi = 0$) up to the limiting streamline. The capture efficiency can thus be estimated as

$$\eta_{DI}(r_p;\epsilon) = q_h(r_p;\epsilon) = -\int_{r=1}^{r=1+r_p} u_\theta(r,\theta_c;\epsilon)\,\mathrm{d}r = \psi(1+r_p,\theta_c;\epsilon). \tag{4.8}$$

Note that by (2.4), the limiting streamline value $\psi(1+r_p,\theta_c;\epsilon)$ is equal to q_h and, therefore, the capture efficiency.

4.4. *Particle capture efficiency: results*

Particle capture was quantified by applying (4.8) to our DNS results for $0.01 \leqslant Re \leqslant 47$. These results bridge the gap between existing low-*Re* theory and higher-*Re* experimental data. We have validated our numerical particle capture efficiency estimates against experiments performed on single cylinders by Palmer *et al.* (2004) and on branched cylindrical structures by Harvey *et al.* (1995). Our results are also compared to those of Shimeta & Koehl (1997), who evaluated the relative contact rates of two sizes of particles with oceanic suspension feeders with cylindrical capturing filaments (they report P_L, the fraction of the total of particles contacting the collector that are of the larger size). For all experimental data, $St < 0.25$, which agrees with the value of St_c found by Phillips & Kaye (1999) for $Re < 1000$. The ratio Λ describes the comparison between our DNS estimates with theory and the available experimental data ($\Lambda = \eta_{numerical}/\eta_{theory}$ for the comparison with theory, $\Lambda = \eta_{numerical}/\eta_{experiment}$ for the comparison with Harvey *et al.* 1995 and Palmer *et al.* 2004, while $\Lambda = P_{Lnumerical}/P_{Lexperiment}$ for the comparison with Shimeta & Koehl 1997). The modelled values of capture efficiency and P_L agree (to within 15 %) with the entire set of experimental values (figure 6), for which $Re \leqslant 47$ and $r_p \leqslant 1.5$. It is interesting that the DNS estimates agree with experiments with particle size ratios of $r_p \sim O(1)$, as typical formulations of direct interception are thought to be inapplicable to particles whose sizes are comparable to that of the collector. As $Re \to 0$, the numerical estimates of capture efficiency match theoretical estimates from the inner asymptotic analytical solution and the creeping flow solution. Random particle size ratios and Reynolds numbers were tested in the range of validity of the low-*Re* theory (presented as a left-pointing triangle and circles in figure 6).

The hybrid approach presented in § 3 (values of a and b taken from (3.1) together with (4.6) and (2.9)) provides an excellent means of estimating the capture efficiency for $Re \leqslant 10$. After applying (4.1) to obtain the maximum angle of capture (figure 5 or (4.6) can also be used for particles of small size ratio), (2.9) and (4.8) yield an estimate of the particle capture efficiency. As shown by the continuous black line in figure 7, the hybrid approach yields identical particle capture efficiencies to the numerical estimates for $Re \leqslant 10$. In contrast, theoretical estimates lose accuracy with increasing Reynolds number and cannot be used for $Re \gtrsim 1$. Our hybrid approach extends the existing low-*Re* theory into a more relevant *Re* range for particle capture in aquatic systems.

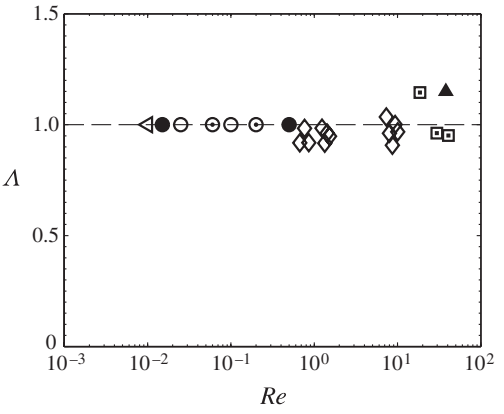

FIGURE 6. The agreement of DNS estimates with theory and experiment. Λ represents the ratio of the DNS estimates to theoretical and experimental values of η and P_L, as explained in the text. The symbols indicate the comparison with: $\triangleleft$, the creeping flow solution; $\bigcirc$, the inner asymptotic analytical solution; $\diamond$, Shimeta & Koehl (1997); $\square$, Harvey *et al.* (1995); and $\triangle$, Palmer *et al.* (2004). The filling of the symbols indicates the particle size ratios: $r_p \leqslant 0.1$ (filled), $0.1 < r_p < 0.5$ (dotted) and $0.5 \leqslant r_p \leqslant 1.5$ (unfilled). For all the experimental data, $St < 0.25$.

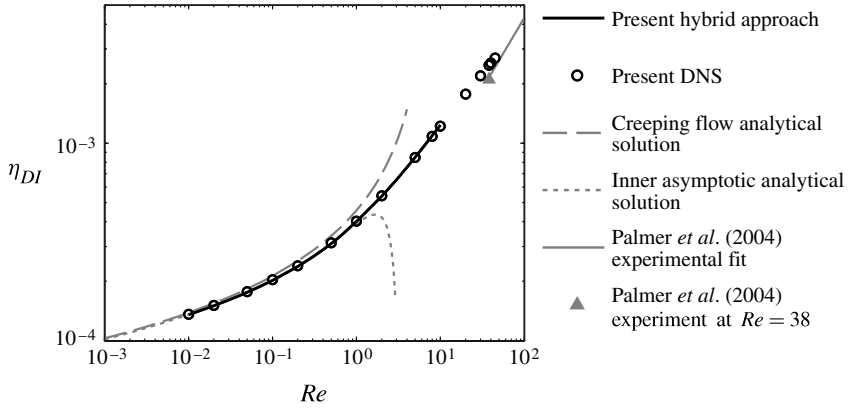

FIGURE 7. The agreement between hybrid approach estimates and DNS estimates of capture efficiency for $Re \leqslant 10$ and $r_p = 0.031$. Analytical expressions are plotted beyond their limit of validity to demonstrate their inaccuracy above $Re = 1$.

The maximum particle size ratio ($r_{p,maxH}$) for which capture efficiency can be estimated using the hybrid approach is dictated by the region in which the flow is accurately described (see § 3.4). For $Re > 1$ the hybrid approach is limited to $r_{p,maxH} \approx 1/\epsilon (\equiv 2/Re)$. The maximum error in capture efficiency estimates from the hybrid approach relative to those from the DNS is 1.5 % across the entire range of validity, i.e. $Re \leqslant 10$ and $r_p \lesssim r_{p,maxH}$.

Particle capture efficiencies are presented graphically for $0.001 \leqslant Re \leqslant 47$ and $0.001 \leqslant r_p \leqslant 1.5$ (figure 8). DNS estimates were complemented with theoretical estimates (the inner asymptotic analytical solution, (2.9) and (2.10)) for $Re < 0.01$. The capture efficiency increases monotonically with both Re and r_p. The dashed lines

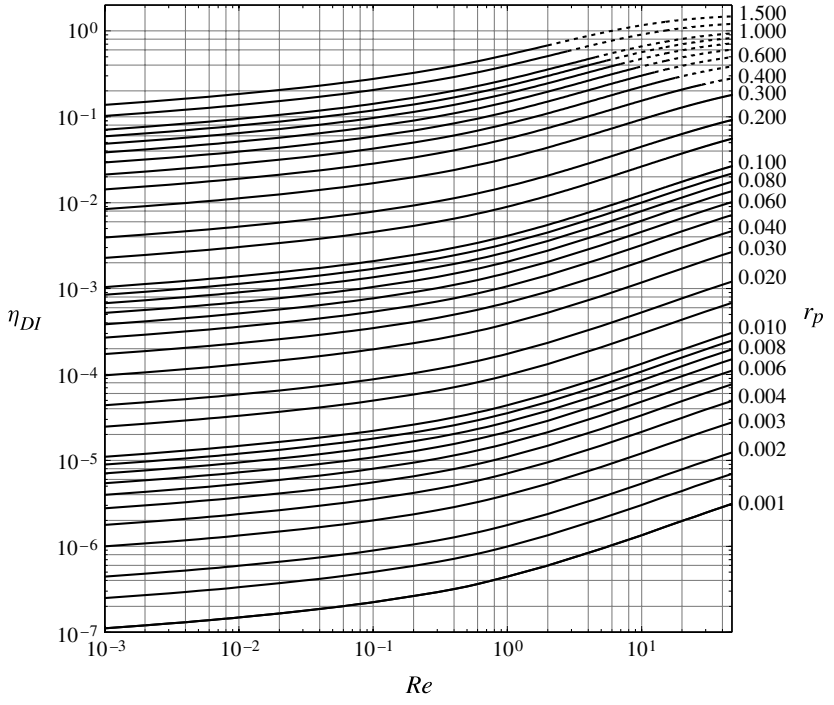

FIGURE 8. Capture efficiency by direct interception (η_{DI}) of a circular cylinder. Re is the Reynolds number based on the diameter of the collector and r_p is the particle–collector radius ratio. Each line corresponds to a particular value of r_p (labelled on the right). Dashed lines represent the region where the Stokes number exceeds 0.25 (for a particle density ratio of $\rho^+ = 1$), such that particle inertia may influence particle capture.

in this figure represent the region where, for $\rho^+ = 1$, the Stokes number exceeds 0.25, the value of St_c estimated by Phillips & Kaye (1999) for $Re < 1000$. Inertial impaction may be non-negligible in this region.

Expressions for particle capture efficiency in creeping flow have previously been obtained by assuming a linear variation of tangential velocity with distance from the cylinder surface (Fuchs 1964; Friedlander 2000). This assumption, together with (4.8), yields an expression of the form

$$\eta_{DI}(r_p, Re) \approx \frac{1}{2}\left(\left.\frac{-\partial u_\theta}{\partial r}\right|_{\substack{r=1\\ \theta=\theta_{c0}}}\right) {r_p}^2, \tag{4.9}$$

which is valid for particles of vanishing size ratio. We propose a similar formulation that is valid for all particle size ratios in the range $0 < r_p \leqslant 1.5$ and over the entire Reynolds number range considered here ($0 < Re \leqslant 47$). This formulation is given by

$$\eta_{DI}(r_p, Re) \approx \underbrace{\frac{1}{2.002 - \ln Re + f(Re)}}_{G(Re)} \underbrace{\frac{{r_p}^2}{(1 + r_p)^{k(Re)}}}_{Y(r_p;Re)}, \tag{4.10}$$

where G is a fit of $(1/2)\,{-}\partial u_\theta/\partial r$ at $(r = 1, \theta = \theta_{c0})$ and Y is a fit of the particle size dependence of the capture efficiency. As the form of (4.10) suggests, the fitting

procedure was actually applied to the auxiliary functions f and k, yielding

$$f(Re) = 0.953\ln(6.25 + Re) - 1.62, \tag{4.11a}$$

$$k(Re) = 0.872\ln(19.1 + Re) - 1.92. \tag{4.11b}$$

The expression in (4.10) (together with (4.11)) provides capture efficiency estimates within 3 % of our DNS estimates (and theory) over the entire particle size ratio and Reynolds number ranges. The reciprocal of G in (4.10) is often termed the 'hydrodynamic factor' (Lee & Gieseke 1980). Its creeping flow form is preserved here, except for the addition of the auxiliary function f, which allows an accurate representation of the maximum gradient of tangential velocity at the cylinder surface over the entire range of Re. The function Y resembles the particle size dependence proposed by Lee & Gieseke (1980) for creeping flow but has been modified such that the exponent in the denominator (k) varies with Re. The approximation $Y \approx r_p^2$ gives an error of less than 5 % when $r_p \leqslant 0.05$ and $Re \leqslant 10$.

5. Conclusions

We have obtained accurate estimates of the rate of capture of suspended particles by cylindrical collectors in the ranges $0 < Re \leqslant 47$ and $0 < r_p \leqslant 1.5$. In doing so, this work fills an existing gap between theoretical and experimental results in particle capture research. The accuracy of the results is confirmed by their agreement with both theoretical estimates at low Re and experimental data at higher Re. The analytical and graphical tools presented here will allow considerable improvement in the prediction of particle capture rates by biological collectors in aquatic systems. Furthermore, our analysis allows us to present, for the first time, a physically based expression for estimating particle capture efficiency for a particle size range relevant to aquatic systems and at all Reynolds numbers below the onset of vortex shedding.

A hybrid approach has allowed the extension up to $Re = 10$ of an inner asymptotic expansion for describing flow around a cylinder (2.9); it has been confirmed that the existing theory is limited to $Re \lesssim 1$. This approach can be used for describing the flow close to the surface of the entire cylinder when $Re \leqslant 1$ and along the frontal face alone when $1 < Re \leqslant 10$, allowing estimation of the capture efficiency and maximum angle of capture with high accuracy. Our hybrid approach is likely to have significant utility for applications that require an analytical description of the flow close to the cylinder surface for $Re \sim O(1\text{–}10)$.

The maximum angle of capture (α_c) over the frontal face of the cylinder coincides with the angle at which the radial velocity changes from negative to positive at a distance equal to the radius of the particle; α_c is less than 90° for $Re \gtrsim 0.001$, a fact that has often been overlooked in analytical studies of particle capture at low Re.

Acknowledgements

A.E.-G. acknowledges the scholarships granted by CONACyT-Banco de México, the Australian Government (IPRS) and The University of Western Australia. The authors are grateful to the iVEC supercomputing facility for the resources granted to this study. This research was supported by an Australian Research Council Discovery Project (DP35603400).

REFERENCES

ACKERMAN, J. D. 1997 Submarine pollination in the marine angiosperm Zostera marina (Zosteraceae). II. Pollen transport in flow fields and capture by stigmas. *Am. J. Bot.* **84** (8), 1110–1119.

ACKERMAN, J. D. 2006 Sexual reproduction of seagrasses: pollination in the marine context. In *Seagrasses: Biology, Ecology and Conservation* (ed. A. W. D. Larkum, R. J. Orth & C. M. Duarte). Springer.

DAVIES, C. N. 1950 Viscous flow transverse to a circular cylinder. *Proc. Phys. Soc. Lond.* B **63** (364), 288–296.

DAVIES, C. N. & PEETZ, C. V. 1956 Impingement of particles on a transverse cylinder. *Proc. R. Soc. Lond.* A **234** (1197), 268–295.

FERZIGER, J. H. & PERIĆ, M. 2002 *Computational Methods for Fluid Dynamics*, 3rd edn. Springer.

FRIEDLANDER, S. K. 1967 Particle diffusion in low-speed flows. *J. Colloid Interface Sci.* **23** (2), 157–164.

FRIEDLANDER, S. K. 2000 *Smoke, Dust and Haze. Fundamentals of Aerosol Dynamics*, 2nd edn. Oxford University Press.

FUCHS, N. A. 1964 *The Mechanics of Aerosols*, 1st edn. Pergamon.

HARVEY, M., BOURGET, E. & INGRAM, R. G. 1995 Experimental-evidence of passive accumulation of marine bivalve larvae on filamentous epibenthic structures. *Limnol. Oceanogr.* **40** (1), 94–104.

HAUGEN, N. E. L. & KRAGSET, S. 2010 Particle impaction on a cylinder in a crossflow as function of Stokes and Reynolds numbers. *J. Fluid Mech.* **661**, 239–261.

HUMPHRIES, S. 2009 Filter feeders and plankton increase particle encounter rates through flow regime control. *Proc. Natl Acad. Sci. USA* **106** (19), 7882–7887.

HUNER, B. & HUSSEY, R. G. 1977 Cylinder drag at low Reynolds number. *Phys. Fluids* **20** (8), 1211–1218.

KAPLUN, S. 1957 Low Reynolds number flow past a circular cylinder. *J. Math. Mech.* **6** (4), 595–603.

KELLER, J. B. & WARD, M. J. 1996 Asymptotics beyond all orders for a low Reynolds number flow. *J. Engng Maths* **30** (1–2), 253–265.

LAMB, H. 1911 On the uniform motion of a sphere through a viscous fluid. *Phil. Mag. Series* 6 **21** (121), 112–121.

LANGE, C. F., DURST, F. & BREUER, M. 1998 Momentum and heat transfer from cylinders in laminar crossflow at $10^{-4} \leqslant Re \leqslant 200$. *Intl J. Heat Mass Transfer* **41** (22), 3409–3430.

LEE, K. W. & GIESEKE, J. A. 1980 Note on the approximation of interceptional collection efficiencies. *J. Aerosol Sci.* **11** (4), 335–341.

OpenFOAM. 2012 http://www.openfoam.com/.

OSEEN, C. W. 1910 Über die Stokes'sche Formel, und über eine verwandte Aufgabe in der Hydrodynamik. *Ark. Mat. Astron. Fys.* **6** (29), 1–20.

PALMER, M. R., NEPF, H. M., PETTERSON, T. J. R. & ACKERMAN, J. D. 2004 Observations of particle capture on a cylindrical collector: implications for particle accumulation and removal in aquatic systems. *Limnol. Oceanogr.* **49** (1), 76–85.

PATANKAR, S. V. 1980 *Numerical Heat Transfer and Fluid Flow*, 1st edn. Taylor and Francis.

PHILLIPS, C. G. & KAYE, S. R. 1999 The influence of the viscous boundary layer on the critical Stokes number for particle impaction near a stagnation point. *J. Aerosol Sci.* **30** (6), 709–718.

POSDZIECH, O. & GRUNDMANN, R. 2007 A systematic approach to the numerical calculation of fundamental quantities of the two-dimensional flow over a circular cylinder. *J. Fluids Struct.* **23** (3), 479–499.

PROUDMAN, I. & PEARSON, J. R. A. 1957 Expansions at small Reynolds numbers for the flow past a sphere and a circular cylinder. *J. Fluid Mech.* **2** (3), 237–262.

RUBENSTEIN, D. I. & KOEHL, M. A. R. 1977 Mechanisms of filter feeding: some theoretical considerations. *Am. Nat.* **111** (981), 981–994.

SEN, S., MITTAL, S. & BISWAS, G. 2009 Steady separated flow past a circular cylinder at low Reynolds numbers. *J. Fluid Mech.* **620**, 89–119.

SHIMETA, J. 1993 Diffusional encounter of submicrometre particles and small-cells by suspension feeders. *Limnol. Oceanogr.* **38** (2), 456–465.

SHIMETA, J. & JUMARS, P. A. 1991 Physical mechanisms and rates of particle capture by suspension-feeders. *Oceanogr. Mar. Biol.* **29**, 191–257.

SHIMETA, J. & KOEHL, M. A. R. 1997 Mechanisms of particle selection by tentaculate suspension feeders during encounter, retention, and handling. *J. Expl Mar. Biol. Ecol.* **209** (1–2), 47–73.

SKINNER, L. A. 1975 Generalized expansions for slow flow past a cylinder. *Q. J. Mech. Appl. Maths* **28** (3), 333–340.

STOKES, G. G. 1851 On the effect of the internal friction of fluids on the motion of pendulums. *Trans. Camb. Phil. Soc.* **9** (Part II), 8–106.

TRITTON, D. J. 1959 Experiments on the flow past a circular cylinder at low Reynolds numbers. *J. Fluid Mech.* **6** (4), 547–567.

VEYSEY, J. & GOLDENFELD, N. 2007 Simple viscous flows: from boundary layers to the renormalization group. *Rev. Mod. Phys.* **79** (3), 883–927.

WILDISH, D. & KRISTMANSON, D. 1997 *Benthic Suspension Feeders and Flow*, 1st edn. Cambridge University Press.

WU, M. H., WEN, C. Y., YEN, R. H., WENG, M. C. & WANG, A. B. 2004 Experimental and numerical study of the separation angle for flow around a circular cylinder at low Reynolds number. *J. Fluid Mech.* **515**, 233–260.